

Interim recruitment prediction for multi-centre clinical trials

Szymon Urbas^{*1}, Chris Sherlock², and Paul Metcalfe³

¹STOR-i Centre for Doctoral Training, Lancaster University, Lancaster, United Kingdom

²Department of Mathematics and Statistics, Lancaster University, Lancaster, United Kingdom

³AstraZeneca, Cambridge, United Kingdom

Abstract

We introduce a general framework for monitoring, modelling, and predicting the recruitment to multi-centre clinical trials. The work is motivated by overly optimistic and narrow prediction intervals produced by existing time-homogenous recruitment models for multi-centre recruitment. We first present two tests for detection of decay in recruitment rates, providing results of a Monto Carlo power study. We then introduce a model based on the inhomogeneous Poisson process with monotonically decaying intensity, motivated by recruitment trends observed in oncology trials. The general form of the model permits adaptation to any parametric curve-shape. A general method for constructing sensible parameter priors is provided and Bayesian model averaging is used for making predictions which account for the uncertainty in both the parameters and the model. The validity of the method, and its robustness to misspecification are tested using simulated datasets. The new methodology is then applied to oncology trial data, where we make interim accrual predictions and indicate where unexpected changes in the accrual pattern occur.

1 Introduction

Efficiently recruiting patients to clinical trials is a critical factor in running clinical trials and hence delivering new medicines to patients as quickly as possible. Late-stage clinical trials are commonly run across many sites, and successfully managing and running trials and subsequent processes requires accurate forecasts of trial recruitment.

Early recruitment rates can be high, for example, because patients with the required condition are already available, and rates can then drop once these patients have been recruited. Deterministic approaches and ad hoc techniques only yield simplified and, often, overly optimistic recruitment timelines, a

^{*}Email: s.urbas@lancaster.ac.uk, Address: STOR-i Centre for Doctoral Training, Lancaster University, Lancaster, United Kingdom

phenomenon thus dubbed *Lasagna's Law* (Lasagna, 1979). In a given trial, 48% of centres failed to enrol the required number of patients in the time originally allocated, leading to extensions of the recruitment timelines and the need to bring more centres into the study, which itself is a costly process (Tufts, 2013). The timelines are usually pushed to nearly twice the originally proposed plan. The most frequent reason for trial discontinuation to be poor recruitment; out of 253 discontinued trials studied in Kasenda et al. (2014), 101 were terminated due to under-recruitment.

This motivates the need for robust statistical methods for modelling and predicting the recruitment to clinical trials. Early detections of possible centre underperformance may allow practitioners to swiftly intervene in the operations. It can also provide realistic timelines for the completion of different stages of the trials.

In this work, we introduce a novel flexible framework for effectively modelling and predicting patient recruitment. We will focus on the oncology therapeutic area as it is known for sparse enrolments whose patterns are not sufficiently captured by the state-of-the-art methods Anisimov and Fedorov (2007); Lan et al. (2018). Our framework utilises time-varying recruitment rates whilst also permitting variation between recruitment centres. Predictions of future recruitment incorporate parameter and model uncertainty, which is essential when data are limited, and are based on a user-specified set of opening times to facilitate the choice between different opening-time scenarios.

As detailed in Section 2, almost all existing multi-centre methods assume time-homogeneity of recruitment rates once a centre has opened. Section 3 outlines methods for detecting recruitment rate decay in the multi-centre recruitment setting along with result of a Monte Carlo power study. Section 4 introduces the flexible modelling framework and Section 5 presents a general method for choosing sensible Bayesian parameter priors, along with an appropriate posterior sampling method and diagnostics. A simulation study is presented in Section 6, illustrating the fitting of the model, model validation and forecasting recruitment using Bayesian model-averaging. In Section 7 the model is fitted to an oncology dataset, and this is followed by a discussion in Section 8.

2 Existing methods

The first statistical modelling framework for clinical trial recruitment was introduced in Lee (1983), where the recruitment was assumed to be a constant-rate Poisson process, leading to tractable inference based on interim data. Williford et al. (1987) built on the model by considering Bayesian inference with conjugate priors. Gajewski et al. (2008) and Jiang et al. (2015) further explored the effects various prior densities can have on predictions. Time-inhomogeneous accrual was first considered in Piantadosi and Patterson (1987), where the aggregated accrual across all sites was modelled as an inhomogeneous Poisson process

with intensity $\lambda(t) = \zeta(1 - e^{-\kappa t})$, $\zeta, \kappa > 0$. [Zhang and Long \(2010\)](#) took a non-parametric approach, using B-splines to model the trends in accrual and using the intensity value at the census time for predictions. [Tang et al. \(2012\)](#) proposed a Poisson model with a piece-wise linear intensity which captured aspects of recruitment such as slow initial recruitment and a spike in recruitment close to the end of the trial. For a more thorough review of these as well as other methods see [Heitjan et al. \(2015\)](#). Accrual-only modelling methods do not consider the effect that opening new centres can have on recruitment trends. For that reason, we shall focus on methods which can take advantage of centre-specific recruitment data.

[Anisimov and Fedorov \(2007\)](#) introduced the Poisson-gamma (PG) model of recruitment in a multi-centre setting, with the main appeal being the use of random effects for the recruitment rates of centres, providing a tractable, data-driven prior predictive distribution for recruitment in yet-unopened centres. The model consists of C centres, each recruiting N_c patients over τ_c days, $c = 1, \dots, C$. The framework makes the following distributional assumptions,

$$\begin{aligned} \lambda_c &\sim \text{Gamma}(\alpha, \alpha/\phi), \\ N_c | \lambda_c &\sim \text{Pois}(\lambda_c \tau_c), \end{aligned} \quad c = 1, \dots, C. \tag{1}$$

The random effect λ_c is the *recruitment rate* for centre c . The rates, and thus the centre recruitments, are assumed to be independent conditional on α and ϕ . There are, however, several caveats with the approach taken. The paper advocates using the Empirical Bayes approach, that is, maximum likelihood estimation for the hierarchical parameters (α, ϕ) followed by re-estimation of the distribution of random effect λ_c given α , ϕ and n_c , for each centre. A method for obtaining the uncertainty in the hierarchical (α, ϕ) parameters is provided, but this uncertainty is not accounted for when making predictions, leading to overly confident prediction intervals. However, the main issue which could result from employing the model arises from the strong assumption of time-homogeneity of centre recruitments, which can lead to underestimations of the time to completion.

Figure 1 shows the accrual in a simulated trial where the rates gradually decay with time as well as the predictive distribution of the PG model fitted at a census time of three-fifths of the total length of the study; the opening day for each centre is marked. The accrual appears to follow a straight line which could initially suggest using a time-homogeneous model. However, new centres are constantly being opened so that a constant recruitment rate for each centre leads to an upward arching trend in accrual. This is encapsulated by the fitted predictive. Here the accrual is initially badly underestimated and then grossly overestimated after the census time. The apparent ‘‘matching’’ at the census time is due to predictions using re-estimated random-effect distributions.

[Lan et al. \(2018\)](#) describes the first multi-centre recruitment model in which the rates decrease over

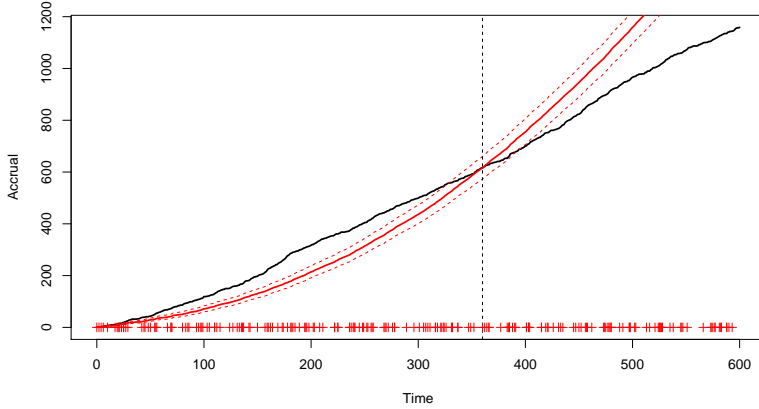


Figure 1: Accrual (black, solid) with the predictive mean (red, solid) and 95% prediction bands (red,dashed), based on the PG model (1) with the census time marked by the vertical, dashed line.

time. The model assumes inhomogenous Poisson for arrivals centre c with an intensity of the form

$$\lambda_c(t) = \begin{cases} \lambda_c^o, & t < t_o \\ \lambda_c^o e^{-\theta(t-t_o)}, & t \geq t_o \end{cases},$$

where λ_c^o is a gamma random effect, as in (1), and t_o is fixed to be six months with no justification given. By enforcing the specific intensity-form, the possibilities of time-homogeneous recruitments or even intensity decays with heavier tails are excluded. A more systematic alternative is to start by testing the time-homogeneity assumption.

3 Detecting time-inhomogeneity

Given series of daily centre recruitment counts over the recruitment period of τ_c days, $\{N_c(t)\}_{t=1}^{\tau_c}$, $c = 1, \dots, C$, we can test the hypothesis of time-homogeneity. To detect a decay in the rate, we only need to use the sums $X_1^{(c)} = \sum_{t=1}^{\tau_c/2} N_c(t)$ and $X_2^{(c)} = \sum_{t=\tau_c/2+1}^{\tau_c} N_c(t)$ ($c = 1, \dots, C$), whose expectations we denote by $\mu_1^{(c)}$ and $\mu_2^{(c)}$ respectively. Detecting time-inhomogeneity in a single centre can be difficult as the infrequent counts will lead to low powers of tests (Krishnamoorthy and Thomson, 2004) (see also Tables 1 and 2). Thus we combine the recruitments across all centres leading to two counts: $X_1 = \sum_{c=1}^C X_1^{(c)}$ and $X_2 = \sum_{c=1}^C X_2^{(c)}$, and we choose our hypotheses to be

$$\mathcal{H}_0 : \sum_{c=1}^C \mu_1^{(c)} = \sum_{c=1}^C \mu_2^{(c)} \quad \text{vs} \quad \mathcal{H}_1 : \sum_{c=1}^C \mu_1^{(c)} > \sum_{c=1}^C \mu_2^{(c)}.$$

The tests are one-sided as we are only interested in recruitment which decays over time. We consider tests with respect to the following assumptions:

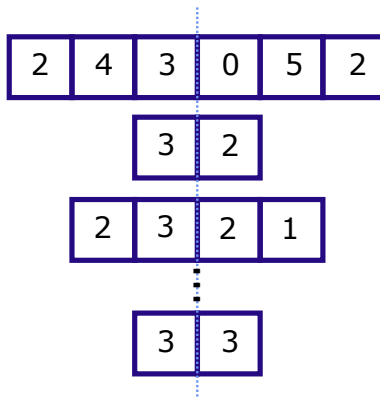


Figure 2: Count series are all centred and the sum of all the first halves is compared to the sum of second halves.

Assumption 1. For each centre $c = 1, \dots, C$, the counts in the first and second halves of that centre's recruitment period are independent and have the same distribution, $X_1^{(c)} \stackrel{d}{=} X_2^{(c)}$, with expectation $\mu_1^{(c)}$. Furthermore, the recruitments at each centre are independent of each other.

Assumption 2. The patients arrive according to a Poisson process such that $X_1^{(c)}, X_2^{(c)} \sim \text{Pois}(\mu_1^{(c)})$, for some $\mu_1^{(c)}$, $c = 1, \dots, C$.

Assumption 1 implies that X_1 and X_2 must have the same distributions, with respective expectations $\mu_1 = \sum_{c=1}^C \mu_1^{(c)}$ and $\mu_2 = \sum_{c=1}^C \mu_2^{(c)}$ being equal. Assumption 2 further implies that the distributions must be Poisson. Figure 2 shows the construction of the quantities X_1 and X_2 by aligning the centres of the recruiting periods. The splitting of the series halfway is arbitrary, though splitting it in half (or at least close to this) would theoretically yield the highest power. It assumes that the τ_c are even. However, centres recruiting over odd numbers of days can still be used by removing the middle day observation. This reduces the power of the tests, though the reduction is negligible.

Gu et al. (2008) offer a detailed Monte Carlo study of the different methods used for testing for a difference in means of two Poisson variables. Here, we focus on the ones most applicable to the clinical-trial recruitment setting, bearing in mind statistical power and robustness. We identified two methods: the non-parametric bootstrapped test (BST), which is powerful yet robust, and the Poisson likelihood-ratio test (LRT), which makes stronger distribution assumptions to achieve an even higher power. The BST only assumes that the counts in each day are independent and identically distributed (Assumption 1). With this assumption, resampling within each centre with replacement, from the original data would still produce a valid sample from the assumed distribution under H_0 . A large number of bootstrap samples is used to simulate the distribution of the difference in two means, which is then used to test the hypothesis. Appendix A details the sampling procedure for obtaining the distribution and the p -value.

For the LRT, we require Assumption 2, which is already an underlying assumption for the model

Table 1: Power for likelihood-ratio test

$\mathbb{E}[X_1]$	$R = 1$	$R = 0.9$	$R = 0.8$	$R = 0.7$	$R = 0.6$	$R = 0.5$
5	0.06	0.08	0.11	0.15	0.20	0.27
10	0.05	0.08	0.12	0.18	0.26	0.37
20	0.05	0.09	0.17	0.27	0.41	0.58
50	0.05	0.13	0.28	0.50	0.73	0.90
100	0.05	0.18	0.44	0.75	0.94	0.99
200	0.05	0.27	0.68	0.95	1.00	1.00

in [Anisimov and Fedorov \(2007\)](#). Upon aggregation, the two sums follow Poisson distributions, that is, $X_1 \sim \text{Pois}(\mu_1)$ and $X_2 \sim \text{Pois}(\mu_2)$. The likelihood under the null model ($\mu_1 = \mu_2$) is compared to the likelihood under the alternative two-mean model ($\mu_1 > \mu_2$). Here, the likelihood function is

$$\mathcal{L}(\mu_1, \mu_2 | x_1, x_2) = \frac{\mu_1^{x_1} e^{-\mu_1}}{x_1!} \frac{\mu_2^{x_2} e^{-\mu_2}}{x_2!}, \quad \mu_1, \mu_2 > 0.$$

We let

$$T_L(x_1, x_2) = \begin{cases} 2[\log \mathcal{L}(\hat{\mu}_1, \hat{\mu}_2 | x_1, x_2) - \log \mathcal{L}(\hat{\mu}, \hat{\mu} | x_1, x_2)], & \hat{\mu}_1 > \hat{\mu}_2 \\ 0, & \hat{\mu}_1 \leq \hat{\mu}_2 \end{cases},$$

where $\hat{\mu}$ is the MLE under the null, and $\hat{\mu}_1$ and $\hat{\mu}_2$ are the MLEs under the alternative hypothesis. Under the null, we would expect the test statistic $T_L(X_1, X_2)$ to asymptotically be zero half the time with the other half following a χ_1^2 distribution. ([Robertson et al., 1988](#)) When using the LRT, the simulated significance levels can differ from the pre-specified level when μ values are low. This is due to using the asymptotic χ^2 distribution when calculating the p -value ([Gu et al., 2008](#)).

The performance of the two tests was assessed by carrying out a Monte Carlo study. Test powers were estimated using Poisson data with different expectations and ratios, $R = \mu_2/\mu_1$. For the LRT power estimates, 5×10^6 samples were used as the test itself is very computationally cheap. For the BST, 5×10^4 samples were used, with each test using a bootstrapped distribution of size 10^3 . Tables 1 and 2 show the results of the study. The biggest difference in powers occurs for lower expectations, with the LRT outperforming BST. It must be noted, however, that the BST only requires the data to be i.i.d. within each centre and thus is robust to violations of the Poisson assumption; if the counts within each centre are overdispersed, for example, it does not affect the Type I error.

Table 2: Power for non-parametric bootstrap test

$\mathbb{E}[X_1]$	$R = 1$	$R = 0.9$	$R = 0.8$	$R = 0.7$	$R = 0.6$	$R = 0.5$
5	0.04	0.06	0.08	0.11	0.14	0.18
10	0.05	0.08	0.12	0.16	0.24	0.33
20	0.05	0.10	0.16	0.25	0.39	0.57
50	0.05	0.14	0.28	0.48	0.70	0.88
100	0.05	0.18	0.42	0.74	0.93	0.99
200	0.05	0.28	0.67	0.94	1.00	1.00

4 Proposed model

We consider a scenario of C centres recruiting patients, with each centre c being open for τ_c days. The number recruited by centre c on day t shall be denoted by $N_c^{(t)}$. We propose the following modelling framework for the multi-centre clinical-trial recruitment, based on the inhomogeneous Poisson process,

$$\begin{aligned}\lambda_c^o &\sim \text{Gamma}\left(\alpha, \frac{\alpha}{\phi}\right), & c = 1, \dots, C, \\ N_c^{(t)} &\sim \text{Pois}\left(\lambda_c^o \int_{t-1}^t g(s; \theta) ds\right), & t = 1, \dots, \tau_c,\end{aligned}$$

where $g : \mathbb{R} \rightarrow [0, \infty)$ dictates the curve-shape of the intensity and θ is a parameter (or parameter vector) associated with the functional form. We use the (α, ϕ) parametrisation for the hierarchical gamma distribution as it leads to orthogonality of α and ϕ in the Poisson-gamma model (Huzurbazar, 1950). *A priori*, $\mathbb{E}[\lambda_c] = \phi$ and $\mathbb{V}[\lambda_c] = \phi^2/\alpha$. For notational simplicity, we define $G(t; \theta) = \int_0^t g(s; \theta) dt$. The likelihood contribution from centre c is

$$\begin{aligned}\mathbb{P}(\mathbf{N}_c = \mathbf{n}_c | \lambda_c^o, \theta, \tau_c) &= \prod_{t=1}^{\tau_c} \mathbb{P}(N_c^{(t)} = n_c^{(t)} | \lambda_c^o, \theta) \\ &= e^{-\lambda_c^o G(\tau_c; \theta)} (\lambda_c^o)^{n_c^{(\cdot)}} \prod_{t=1}^{\tau_c} \frac{[G(t; \theta) - G(t-1; \theta)]^{n_c^{(t)}}}{n_c^{(t)}!},\end{aligned}$$

where $n_c^{(\cdot)} = \sum_{t=1}^{\tau_c} n_c^{(t)}$. Marginalising over the random-effect component gives

$$\mathbb{P}(\mathbf{N}_c = \mathbf{n}_c | \alpha, \phi, \tau_c) = \frac{(\alpha/\phi)^\alpha \Gamma(\alpha + n_c^{(\cdot)})}{\Gamma(\alpha) [G(\tau_c; \theta) + \alpha/\phi]^{(\alpha + n_c^{(\cdot)})}} \prod_{t=1}^{\tau_c} \frac{[G(t; \theta) - G(t-1; \theta)]^{n_c^{(t)}}}{n_c^{(t)}!},$$

whence the full likelihood of the model given the recruitment data is:

$$\begin{aligned}\mathcal{L}(\alpha, \phi, \theta | \mathbf{n}, \tau) &= \prod_{c=1}^C \mathbb{P}(\mathbf{N}_c = \mathbf{n}_c | \alpha, \phi, \tau) \\ &= \frac{(\alpha/\phi)^{C\alpha}}{\Gamma(\alpha)^C} \prod_{c=1}^C \frac{\Gamma(\alpha + n_c^{(\cdot)})}{[G(\tau_c; \theta) + \alpha/\phi]^{(\alpha + n_c^{(\cdot)})}} \prod_{t=1}^{\tau_c} \frac{[G(t; \theta) - G(t-1; \theta)]^{n_c^{(t)}}}{n_c^{(t)!}}.\end{aligned}\quad (2)$$

If all the centres had been open for the same amount of time, that is, $\tau_c \equiv \tau \forall c$, then by fixing the integral of $g(t; \theta)$ over τ days we could introduce orthogonality between (α, ϕ) and θ by imposing the normalisation: $\int_0^\tau g(t; \theta) dt = \tau$. This generalises a homogeneous model with $g(t; \theta) = 1$ and leads to the following factorisable likelihood,

$$\begin{aligned}\mathcal{L}(\alpha, \phi, \theta | \mathbf{n}, \tau) &= \frac{(\alpha/\phi)^{C\alpha}}{\Gamma(\alpha)^C (\tau + \alpha/\phi)^{(C\alpha + n_\Sigma)}} \prod_{c=1}^C \Gamma(\alpha + n_c^{(\cdot)}) \prod_{t=1}^{\tau_c} \frac{[G(t; \theta) - G(t-1; \theta)]^{n_c^{(t)}}}{n_c^{(t)!}} \\ &= \mathcal{L}(\alpha, \phi | \mathbf{n}, \tau) \mathcal{L}(\theta | \mathbf{n}, \tau),\end{aligned}\quad (3)$$

where $n_\Sigma = \sum_{c=1}^C n_c^{(\cdot)}$.

The factorisation means that now the θ parameter describes the shape of the intensity only, and α and ϕ describe the distribution of the magnitude of the integrated intensity, leading to a more interpretable model.

Even when centres are not all open the same length of time, we choose to impose a similar normalisation using some representative τ , here $\frac{1}{C} \sum_{c=1}^C \tau_c$. As demonstrated empirically in Section 6, the condition leads to approximate orthogonality even when the centres are opened uniformly throughout the study.

4.1 Intensity curve-shape

In this work, we will restrict our choice of curve-shape g to parametric forms. The functional form of g is arbitrary and the best choices may depend on the context of the problem. When working with oncology datasets, we observe low-frequency counts which seem to become even less frequent over time but with varying tail behaviours. For this reason, we chose the following curve-shape

$$g_\kappa(t; \theta) \propto \left(1 + \frac{\theta t}{\kappa}\right)^{-\kappa}, \quad t \geq 0, \quad \theta, \kappa > 0. \quad (4)$$

The limit as $\kappa \rightarrow 0$ recovers the standard PG model (1); and letting $\kappa \rightarrow \infty$, we obtain an exponential tail. The full (normalised) forms are then

$$g_0(t) \equiv 1, \tag{5}$$

$$g_1(t; \theta) = \frac{\theta(1 + \theta t)^{-1}}{\log(1 + \theta\tau)} \tau, \tag{6}$$

$$g_\kappa(t; \theta) = \frac{\theta(1 - \kappa)(1 + \theta t/\kappa)^{-\kappa}}{\kappa(1 + \theta\tau/\kappa)^{1-\kappa} - 1} \tau, \quad \kappa \notin \{0, 1, \infty\}, \tag{7}$$

$$g_\infty(t; \theta) = \frac{\theta e^{-\theta t}}{1 - e^{-\theta\tau}} \tau. \tag{8}$$

The associated integrated forms, $G_\kappa(t; \theta)$ are provided in Appendix B.

The flexibility of the model, however, can result in potential identifiability issues. Inference methods, such as maximum likelihood, can run into numerical instabilities when $\kappa \gg 1 > \theta$ or $\kappa < 1 \ll \theta$ (see the Supplementary Material for details). For this reason, we recommend restricting the choice of κ to a discrete set of values; in this work, we use $\{0, 0.5, 1, 2, \infty\}$. This will be elaborated on in Section 5.3.

5 Inference, diagnostics and predictions

We aim to construct a framework which can provide reliable predictions whilst capturing uncertainty in the estimated parameters and in the underlying model itself. We employ the Bayesian paradigm since it naturally incorporates the distribution of the random effects, λ_c , with the uncertainty in the model and the parameter values. However, we note that in some scenarios frequentist methods may be preferred and give a brief outline of how one may employ them in Appendix C.

Given a parametric statistical model the Bayesian paradigm starts from a prior distribution for the parameters, here denoted $\pi_0(\alpha, \phi, \theta)$ and updates this according to some data, y , to provide a posterior distribution, here denoted by $\pi(\alpha, \phi, \theta|y)$. When multiple parametric models, \mathcal{M}_k , $k = 1, \dots, K$, are being considered, the posterior probability for model k , here denoted by $\pi_p(\mathcal{M}_k|y)$, may also be calculated. Section E of the supplementary material provides more details on these quantities; see also Robert and Casella (2013) or Gelman et al. (2013), for example.

For the models under consideration for trial-recruitment data, neither the posterior model probabilities nor the posteriors for the parameters for any particular model are tractable, and so we employ importance sampling to obtain Monte Carlo samples $(\alpha_m, \phi_m, \theta_m)$, $m = 1, \dots, M$ from the posterior distribution for any given model, as well as an estimate of $\pi(\mathcal{M}_k)$, $k = 1, \dots, K$. Section E of the supplementary material provides further details of this method, as well as of effective sample size (ESS), a diagnostic which indicates the reliability of the Monte Carlo estimates; see also Robert and Casella (2013) or Smith

(2013).

In Sections 6 and 7, we carry out inference on $\tilde{\alpha} = \log \alpha$, $\tilde{\phi} = \log \phi$ and $\tilde{\theta} = \log \theta$ since analyses of trial data showed the likelihood in the log-parameters to be more symmetric about the mode, which can make sampling more efficient. For the importance sampling proposal distribution, we use a multivariate t -distribution on 4 degrees of freedom, with the same mode as the posterior and the shape matrix equal to the inverse Hessian at the posterior mode.

5.1 Prior choices

We base our prior specification on a maximum likelihood meta-analysis of 20 oncology clinical trial recruitment datasets. In all cases, the parameter estimators were close to orthogonal justifying the use of independent priors: $\pi_0(\tilde{\alpha}, \tilde{\phi}, \tilde{\theta}) = \pi_0(\tilde{\alpha})\pi_0(\tilde{\phi})\pi_0(\tilde{\theta})$.

We found that the α parameter does not change much from one study to another. The prior $\tilde{\alpha} \sim \mathcal{N}(0.2, 2^2)$ sufficiently reflects the distribution of the estimated values.

The ϕ parameter estimates varied by orders of magnitude between studies. The parameter reflects the mean centre recruitment and is well identified by the data; it depends upon the catchment region, type of indication and protocol, for example. For this reason, we advocate using a vague prior unless reliable expert knowledge is available. In our analyses, we used the uninformative, proper prior $\tilde{\phi} \sim \mathcal{U}(-8, 8)$.

The difference between the homogeneous (5) and the inhomogeneous (6,7, 8) models is the curve-shape parameter θ . Lindley’s paradox (Lindley, 1957) warns that assigning θ a vague prior can lower the posterior probabilities of the models that use θ , compared to the model with $\kappa = 0$ which does not use θ . To avoid the paradox we set an informative but sensible prior by considering the drop off in intensity after some time, t_0 . We let $R = g(t_0; \theta)/g(0; \theta)$ and set $R \sim \text{Beta}(a, b)$ *a priori*, with $a = b = 1.1$ to indicate a lack of information, excepting that this is not a constant intensity model, since this is covered by $\kappa = 0$, and that we do not expect a 100% drop off after a time of t_0 (expert opinion); here we take $t_0 = 4$ months. As R is a monotonic function of θ , we can use a density transform to derive the corresponding prior for θ . If prior information is abundant, be it in the form of historical data or expert knowledge, the beta distribution parameters can be adjusted to reflect this. Given (4), the resulting prior density for $\tilde{\theta}$ is given in Appendix D.

5.2 Predictive distribution

There are two complementary properties for which predictions might be required: the distribution of future recruitments within a set time interval, and the distribution of time until the target number of recruitments is reached. In this section, we focus on the former; details of the latter appear in Appendix

E.

Suppose we are interested in sampling the recruitment, denoted N_c^+ , at some day t^+ by centre c . Given samples from the parameter posteriors, we can sample exactly from the posterior predictive for N_c^+ by exploiting the Poisson-gamma conjugacy of the random-effect distribution. The posterior distribution for the λ_c^o random effect for centre c is

$$\lambda_c^o | \alpha, \phi, \theta, \mathbf{n}_c, \tau_c \sim \text{Gamma} \left(\alpha + n_c^{(\cdot)}, \alpha / \phi + G(\tau_c; \theta) \right) = \text{Gamma} \left(\alpha_c^*, \frac{\alpha_c^*}{\phi_c^*} \right), \quad (9)$$

where $\alpha_c^* = \alpha + n_c^{(\cdot)}$ and $\phi_c^* = \phi \times \left(\frac{\alpha + n_c^{(\cdot)}}{\alpha + \phi G(\tau_c; \theta)} \right)$. The predictive distribution for N_c^+ conditional on the random effect is:

$$N_c^+ | \lambda_c^o, \theta \sim \text{Pois} \left(\lambda_c^o \int_{t^+-1}^{t^+} g(s; \theta) ds \right) = \text{Pois} (\lambda_c^o G_\theta^+), \quad (10)$$

where $G_\theta^+ = \int_{t^+-1}^{t^+} g(s; \theta) ds$.

Marginalising over the random effect posterior, we arrive at the negative binomial distribution:

$$\mathbb{P}(N_c^+ = n | \alpha_c^*, \phi_c^*) = \frac{\Gamma(\alpha_c^* + n)}{\Gamma(\alpha_c^*) n!} \left(\frac{\alpha_c^*}{\alpha_c^* + \phi_c^* G_\theta^+} \right)^{\alpha_c^*} \left(\frac{\phi_c^* G_\theta^+}{\alpha_c^* + \phi_c^* G_\theta^+} \right)^n, \quad n \in \mathbb{N}. \quad (11)$$

The length of interval to t^+ does not need to be a day and could instead be a week or a month, depending on the context of the application. To obtain the full marginal predictive, we sample the recruitments conditional on parameters sampled from the posterior. For as yet unopened centres, we set $n_c^{(\cdot)} = \tau_c = 0$. For each triplet (or couplet, if $\kappa = 0$) of parameters sampled from the posterior, we sample N_c^+ , $c = 1, \dots, C$, and sum them to obtain a sample from $N^+ | \alpha, \phi, \theta$. The collection of these sums is a sample from the posterior predictive distribution for the model.

If simulations for multiple distinct time periods are required for a given centre, c , as needed for the accrual curve for example, then we first sample λ_c^o from its posterior (9). We then simulate the Poisson counts for the individual time periods, which are conditionally independent given λ_c^o , from (10).

5.3 Model averaging

When predicting the enrolments using a fitted model, we implicitly assume that a single model best reflects reality; however, prediction methods should consider the uncertainty in the models used for inference. We shall, therefore, use model averaging for making predictions, that is, take a weighted average of predictions made by each model. Working in the Bayesian paradigm provides us with an intuitive choice for weights in the form of marginal likelihoods of the models.

$$\mathbb{P}(N^+ = n^+ | \mathbf{n}, \tau) = \sum_{k=1}^K \mathbb{P}(N^+ = n^+ | \mathbf{n}, \tau, \mathcal{M}_k) \pi_p(\mathcal{M}_k | \mathbf{n}, \tau),$$

where

$$\pi_p(\mathcal{M}_k|\mathbf{n}, \tau) \propto \pi(\mathbf{n}|\tau, \mathcal{M}_k)\pi_0(\mathcal{M}_k), \quad k = 1, \dots, K,$$

with $\pi_0(\mathcal{M}_k)$ being prior model probabilities. The averaging framework fits in with the restriction of the shape parameter κ to a discrete space. Each κ value generates an inhomogeneous Poisson-gamma model with the tail behaviour of the associated intensity shape. This includes the null ($\kappa = 0$) model as in [Anisimov and Fedorov \(2007\)](#). In this work we set all prior model probabilities equal.

5.4 Model validation

Before making any statements in regards to the future recruitments, we should validate that the fitted model does indeed capture the true data-generating process sufficiently well. Since the true process is unknown, we compare the observed data to the modal model (the model with the highest posterior probability) fixed at posterior parameter means $(\hat{\alpha}, \hat{\phi}, \hat{\theta})$.

Firstly, we wish to assess that the chosen hierarchical structure is reflected in the data. The distribution of posterior means of the individual random effects should approximately follow the hierarchical $\text{Gamma}(\hat{\alpha}, \hat{\alpha}/\hat{\phi})$ distribution. A QQ-plot can be used to visually compare the distributions. If deemed sufficiently similar, using the distribution for generating predictions for yet-unopened centres is appropriate. If the distributions are noticeably different, particularly if the true distribution is multimodal, any interim predictions for yet-unopened centres could be inaccurate.

According to the model, the counts in any initial period $[0, t_*]$ (such as the first month) of each centre's recruitment period, follow a negative binomial distribution as in (11) but with $G_\theta^+ = \int_0^{t_*} g(t; \theta) dt$, and $(\hat{\alpha}, \hat{\phi}, \hat{\theta})$ used instead of $(\alpha^*, \phi^*, \theta)$. We use the prior random effect distributions for each recruitment rate so that the diagnostic indicates if the combination of the gamma random effects and the modal decay model captures well the behaviour over in the initial period after a centre has been opened. Again, a QQ-plot can be used for comparing the theoretical distribution to the observation, giving an indication if the fitted model under- or overestimates initial recruitment. The initial period, $[0, t_*]$, should be long enough that the true recruitment decay should be apparent. However, since only centres that have been open for a period of at least t_* can be used for the diagnostic, to ensure a reasonable power, t_* should be short enough that a large number of sites have been recruiting for this duration. In this work, we set $t_* = 60$ (2 months).

5.5 Assessing forecast accuracy

The predictive distribution can be used to forecast future accrual from the census time. Here, a statistic for assessing the accuracy of the forecast is provided. We choose the statistic to be the maximum of the standardised deviation from the predictive mean of the accrual. Let $\mathbf{A} = \{A_t\}_{t=\tau+1}^{\tau^H}$ be the accrual from the census time τ up to some horizon τ^H . Defining an index set $\mathcal{T} = \{\tau + 1, \dots, \tau^H\}$, we construct a statistic

$$T(\mathbf{A}) = \max_{t \in \mathcal{T}} \frac{|A_t - \mathbb{E}[A_t]|}{\sqrt{\mathbb{V}[A_t]}},$$

where the moments of A_t are obtained by averaging the (tractable) moments of the negative binomial distributions (11) over the parameter samples within each model and weighting according to the posterior model probabilities. Using the samples from the posterior predictive, we can obtain the distribution of $T(\mathbf{A})$ and examine how much the true future accrual, \mathbf{A}^{obs} , deviates from the model predictive via the forecast p -value $\mathbb{P}(T(\mathbf{A}) \geq T(\mathbf{A}^{obs}))$. The p -value represents the extent to which the newly observed data fits with the posterior predictive from the fitted model, values close to 0 and 1 indicating poor fit. Since the posterior predictive is also used to predict beyond τ^H , this provides a measure of the trustworthiness of such further forecasts.

6 Simulation results

We demonstrate our flexible framework through a simulation study, using simulated data sets to illustrate model fit and prediction and to highlight the effect model misspecification can have on predictions.

We simulate a study over a course of 600 days, with 200 centres, opening uniformly in the time interval. The parameters used for simulations were $\alpha = 1.4$, $\phi = 0.01$, $\kappa = 2.7$ and $\theta = 0.02$. Figure 3 shows the simulated accrual. The inference is carried out on data observed in the first 360 days. As motivated in Section 1, and in contrast to Lan et al. (2018), we assume the opening times to be known by the practitioner. We consider a set of models with flexible tails (Section 4.1) allowing $\kappa \in \{0, 0.5, 1, 2, \infty\}$, thus including the null model (Anisimov and Fedorov, 2007). The “normalisation” of the curve-shapes was imposed at $\tau = \frac{1}{C} \sum_{c=1}^C \tau_c$. We purposely simulated using a κ value outside of those considered in our models to illustrate the flexibility of the framework. For Bayesian inference, we used parameter and model priors outlined in Sections 5.1 and 5.3 respectively. Based on the model fitted to the data at the census day 360, we wish to predict the daily accrual until day 600.

Performing the LRT and BST from Section 3, we find the p -values of both tests to be < 0.001 . Table 3 provides the fits for the five models. The effective samples sizes are high, which means that each of the model posteriors is represented well by its respective sample and that the marginal likelihood

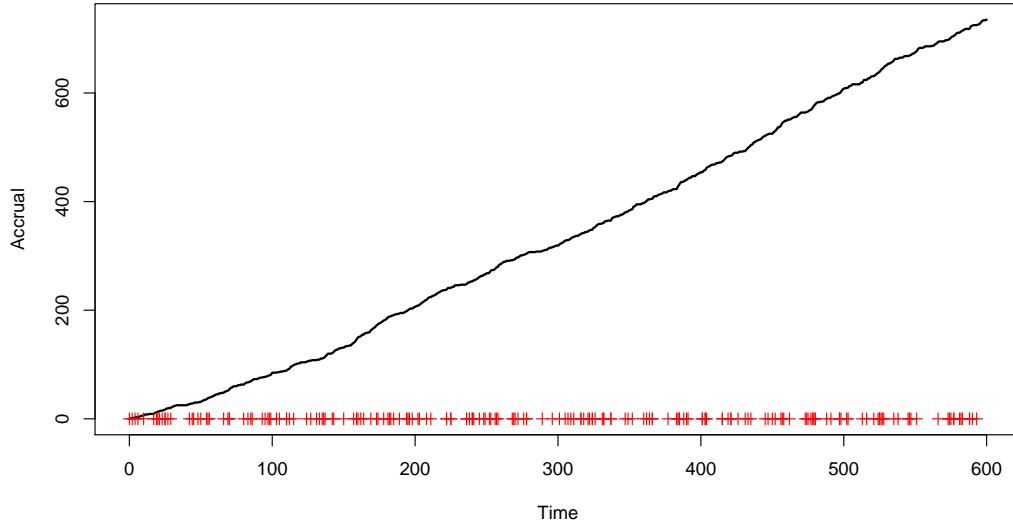


Figure 3: Accrual plot with the centre opening times marked by “+” symbols on the abscissa.

κ	α	ϕ	θ	$\pi(\mathcal{M}_k \mathbf{n})$	ESS
0	1.141 (0.771, 1.672)	0.013 (0.011, 0.017)	--	3.49×10^{-25}	9006
0.5	1.167 (0.759, 1.745)	0.013 (0.010, 0.016)	0.143 (0.044, 0.441)	5.51×10^{-4}	8519
1	1.144 (0.742, 1.744)	0.013 (0.011, 0.016)	0.033 (0.021, 0.049)	2.21×10^{-1}	8665
2	1.142 (0.728, 1.644)	0.014 (0.011, 0.016)	0.017 (0.012, 0.023)	6.58×10^{-1}	8564
∞	1.122 (0.718, 1.645)	0.014 (0.011, 0.017)	0.009 (0.007, 0.011)	1.20×10^{-1}	8610

Table 3: Posterior means and 95% credible intervals, posterior model probabilities and effective sample sizes, obtained using 10^4 importance samples for each model.

estimates are accurate. If the ESS values had been low, we would have retried using more samples in the importance sampler. We see that model corresponding to $\kappa = 2$ has the highest posterior probability. A trellis plot of the posteriors for $(\tilde{\alpha}, \tilde{\phi}, \tilde{\theta})$ from the modal model (see Supplementary material) confirms at least approximate pairwise orthogonality between the parameters, as anticipated from Sections 4 and 5.1. QQ-plots for the modal model comparing the hierarchical gamma distribution to the posterior means of the random effects, and comparing the observed recruitments over the first two months of each centre’s opening to the model’s negative binomial distribution both show approximate straight lines with unit gradient and are provided in the Supplementary Material.

Figure 4 shows the accrual forecast from the census time $\tau = 360$ up to the horizon $\tau^H = 600$, superimposed onto the true accrual plot. The forecast is based on the Bayesian model-averaged posterior predictive distribution. The true accrual is contained within the 95% predictive intervals. In this example, we found the p -value over the forecasting period to be 0.876.

Figure 5 uses an earlier census time ($\tau = 240$) to illustrate the issues that can arise when making predictions using maximum likelihood estimation and model selection. The inference was carried out with the same set of candidate models, and predictions were obtained by simulating from the best model ($\kappa = 2$, chosen using AIC) with parameters fixed at the MLEs. As shown in the plots, not accounting for parameter and model uncertainty may lead to overly confident and biased predictions. Simulations with $\tau = 360$ (see Supplementary material) still showed bias due to the choice of a single model, although the contrast with Figure 4 in terms of prediction interval width was less marked.

We repeated the analysis with a different distribution of opening times, making the centre initiations “clump” roughly every two months. The resulting forecast predictive distribution can be seen in Figure 6, with the forecast p -value=0.611; performance appears to be robust to the type of opening schedule.

To further test the robustness of the framework, we first consider the random effects λ_c^o now being generated from a mixture of two gamma distributions

$$\lambda_c^o | \alpha, \phi_1, \phi_2 \sim \frac{1}{2} \text{Gamma} \left(\alpha, \frac{\alpha}{\phi_1} \right) + \frac{1}{2} \text{Gamma} \left(\alpha, \frac{\alpha}{\phi_2} \right).$$

We considered data generated using the same α value and curve-shape as before. The ratio of gamma expectations was fixed such that $\phi_2 = 10\phi_1$, and the random effect expectation, $\mathbb{E}[\lambda_c^o] = (\phi_1 + \phi_2)/2$, was set to 0.01 and then 0.03. Figure 7 shows example forecasts for accruals with the two different expectations. The more data, that is, the larger $\mathbb{E}[\lambda_c^o]$, the more apparent the discrepancy in the random-effect distribution, and the concomitant predictions, becomes. This is visible in the clearly non-linear diagnostic QQ-plots, the prediction p -values, and the plotted forecasts (see Supplementary Material). The robustness of predictions comes from the fact that the random effects for opened centres use re-

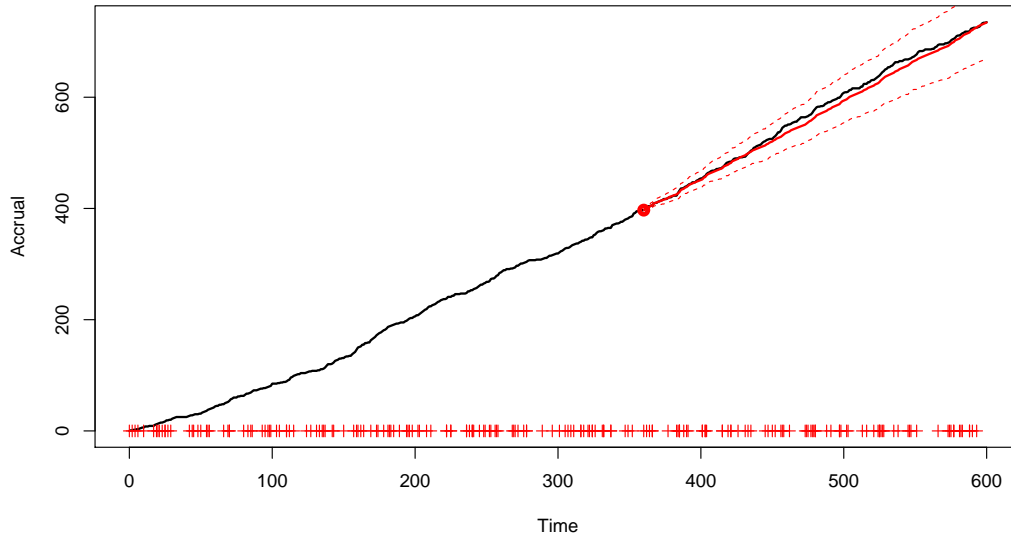
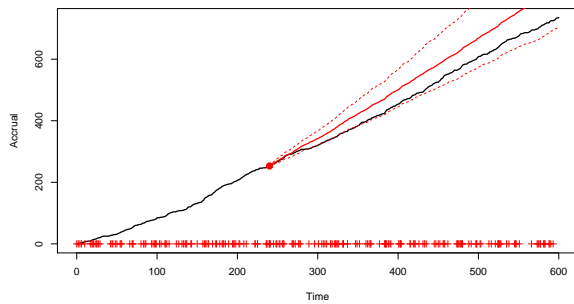
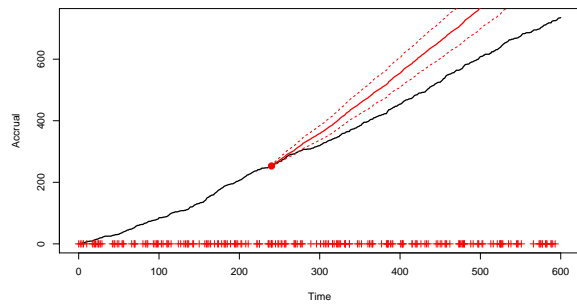


Figure 4: Accrual with Bayesian model-averaged forecast predictive mean (solid, red) and 95% prediction bands (red, dashed). Prediction bands are based on the 2.5% and 97.5% quantiles. The forecast begins from a point marked by the red dot and the “+” symbols on the abscissa indicate centre opening times.



(a) Bayesian model averaging



(b) Maximum likelihood and model selection

Figure 5: Comparison of accrual predictions produced by two methods; accruals (black, solid) with predictive means (red, solid) and 95% prediction bands (red, dashed). Prediction bands are based on the 2.5% and 97.5% quantiles. The “+” symbols on the abscissa indicate centre opening times.

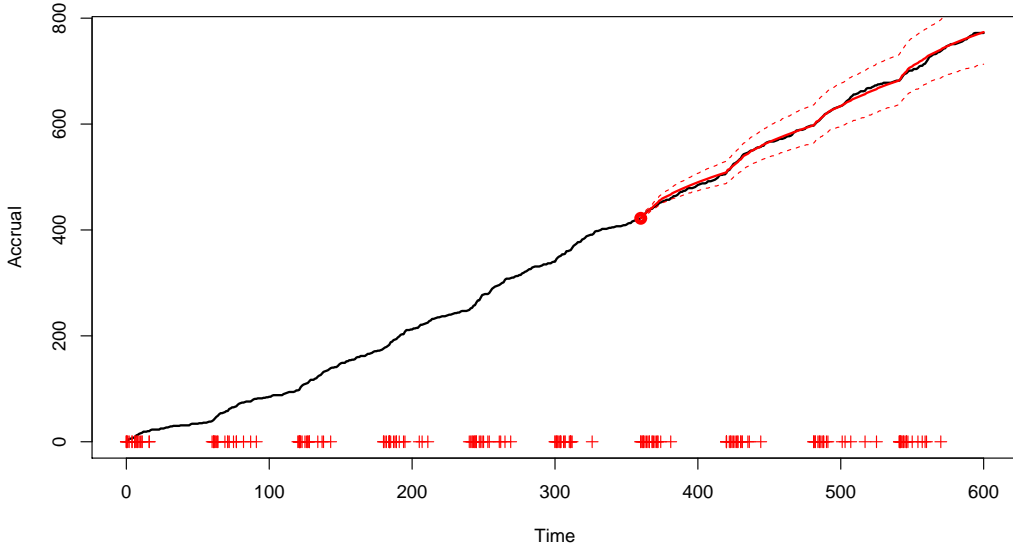


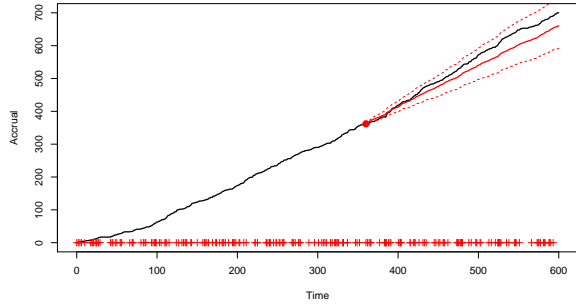
Figure 6: Accrual with forecast predictive mean (solid, red) and 95% prediction bands (red, dashed). Prediction bands are based on the 2.5% and 97.5% quantiles. The forecast begins from a point marked by the red dot and the “+” symbols on the abscissa indicate centre opening times.

estimated data-driven distributions, reducing the importance of the random-effect prior; thus the main source of forecasting error comes from the incorrect random-effect prior for new centres. Similar plots for the “clumped” opening schedule, provided in the Supplementary material, show the same pattern. This mixture distribution of random effects represents the (extreme) scenario where roughly half of the centres recruit the vast majority of patients, with the remaining sites recruiting little to none each. When the ratio of the two means is closer to 1, the model still produces reliable predictions.

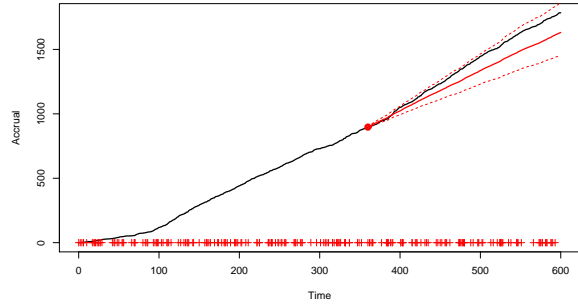
We also consider the effect of curve-shape misspecification on predictions, generating data using an intensity proportional to the Weibull density function

$$g_W(t; \theta, k) = \frac{\frac{k}{\theta} \left(\frac{t}{\theta}\right)^{k-1} e^{-(t/\theta)^k}}{1 - e^{-(\tau/\theta)^k}} \tau, \quad \text{so} \quad G_W(t; \theta, k) = \frac{1 - e^{-(t/\theta)^k}}{1 - e^{-(\tau/\theta)^k}} \tau,$$

where $\theta, k > 0$. We simulated accrual datasets using the Weibull shape with $\theta = 30$ and $k = 1.5$, resulting in the highest recruitment rates occurring two weeks after centre initiation. The random-effect distribution used $\alpha = 1.4$ and two different values ϕ were used: 0.01 and 0.03. Figure 8 shows example forecasts. For lower overall recruitment levels, the model still predicts future accrual well. Forecast inaccuracies due to model misspecification become more apparent when larger recruitment rates are used. The same pattern is observed when centre opening times are clumped (see Supplementary Material).

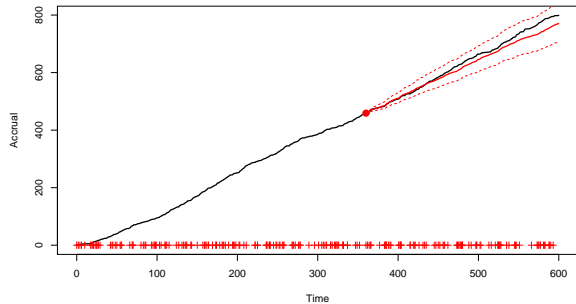


(a) Uniform openings, $\mathbb{E}[\lambda_c^o] = 0.01$;
 p -value = 0.212

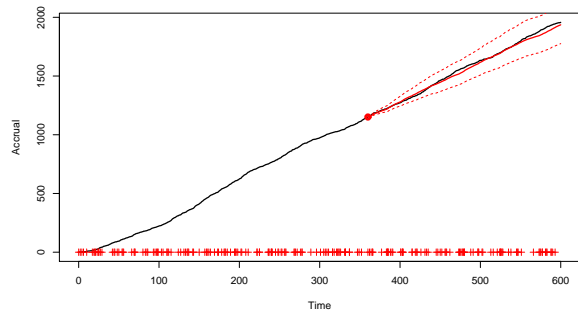


(b) Uniform openings, $\mathbb{E}[\lambda_c^o] = 0.03$;
 p -value = 0.207

Figure 7: Accruals (black, solid) with predictive means (red, solid) and 95% prediction bands (red, dashed) when the true random-effect distribution is a mixture. Prediction bands are based on the 2.5% and 97.5% quantiles. The “+” symbols on the abscissa indicate centre opening times.



(a) Uniform openings, $\mathbb{E}[\lambda_c^o] = 0.01$;
 p -value = 0.553



(b) Uniform openings, $\mathbb{E}[\lambda_c^o] = 0.03$;
 p -value = 0.033

Figure 8: Accruals (black, solid) with predictive means (red, solid) and 95% prediction bands (red, dashed) when the true intensity shape is Weibull, for two different values of $\mathbb{E}[\lambda_c^o]$. Prediction bands are based on the 2.5% and 97.5% quantiles. The “+” symbols on the abscissa indicate centre opening times.

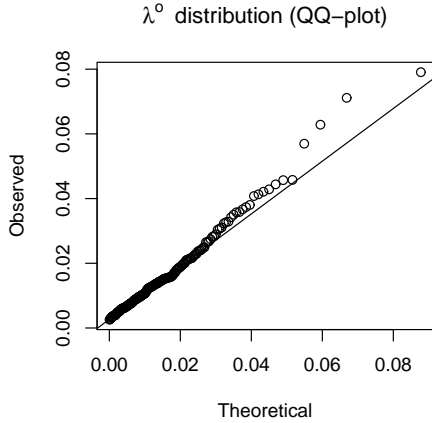


Figure 9: Re-estimated λ_c^o expectations compared to Gamma($\hat{\alpha}, \hat{\alpha}/\hat{\phi}$) distribution.

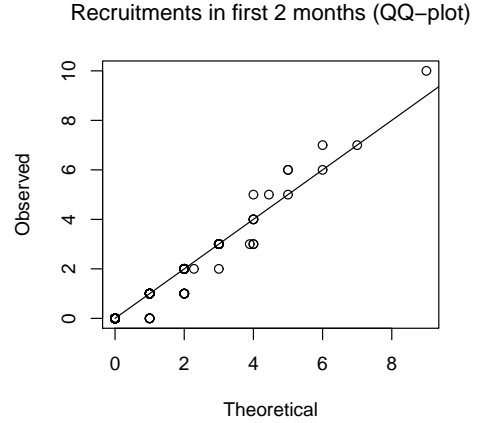


Figure 10: Observed recruitments compared to the theoretical negative binomial distribution.

Census time	BST p -value	LRT p -value	Forecast p -value
1	0.196	0.226	0.697
2	0.012	0.021	0.625
3	< 0.001	< 0.001	0.029
4	< 0.001	< 0.001	< 0.001

Table 4: Decay in rate test p -values and the forecasting p -values at four census times.

7 Data results

We fitted the same set of models to a recruitment dataset of a prostate-cancer clinical trial. The recruitment was carried out across 244 sites. The accrual is presented as the proportion of the total number enrolled. Similarly, the time represents the proportion of the recruiting period. Figures 9 and 10 show the diagnostic QQ-plots for the model fitted to data available at time 0.4. They indicate that there is sufficient concordance between the assumed model and observed enrolment giving validity to potential predictions. Figure 11 shows the accrual along with forecasts from four different census times. The predictive bands become narrower, and parameter uncertainty decreases, at each census as more data become available for inference. Near the end of the trial, at the final census time, there is an unexpected global drop in recruitment, probably indicating a global external factor, such as a change in the protocol. This unexpected change is reflected by the drop of the forecast p -value as indicated in Table 4. The forecast p -values are calculated for the whole rest of the recruitment period. The table also shows p -values of the LRT and BST. Initially, when the accrual is still only a small proportion of the total, it is hard to detect the time-inhomogeneity. At later census points, the test outcomes indicate that the rates are not constant.

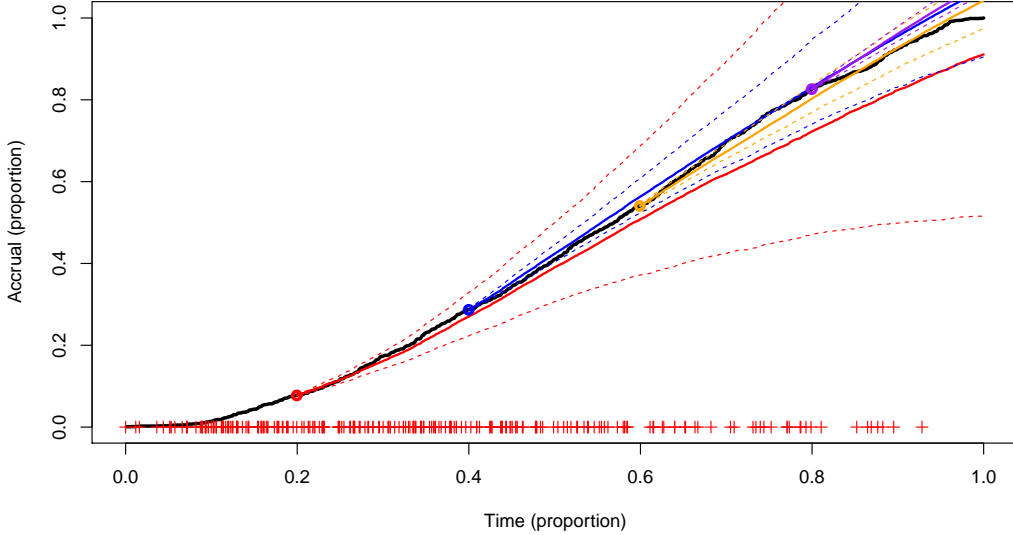


Figure 11: Accrual (black, solid) for an oncology study; coloured solid lines are mean predictions from census times, dashed lines are the 95% prediction bands, and the “+” symbols indicate opening times of centres.

8 Discussion

We have introduced a general, flexible framework for modelling and predicting recruitment to clinical trials. We suggest two tests for detecting decay in recruitment rates; comparing them both with respect to power and robustness. The parametric curve-shape forms chosen for the intensity were based on the features encountered in oncology trials. We found that the model was still robust to moderate model misspecifications in the distribution of the random effect and intensity shape. Other therapeutic areas such as pulmonary or cardio-vascular diseases experience more frequent recruitments and different curve-shapes may be appropriate. As shown in Section 6, model misspecification becomes more of a problem at larger enrollment rates. However, with increased frequency, pattern changes in the early months of a centre are easier to identify. Using more complex parametric forms, such as the generalised gamma shape, could lead to more accurate predictions. Alternatively, if covariate information is available, say $\mathbf{x}_c \in \mathbb{R}^d$ for each centre, the following intensity form motivated by hazard models from survival analysis could be used

$$\lambda_c(t) = \lambda_c^o e^{\beta^\top \mathbf{x}_c} g\left(t; e^{\eta^\top \mathbf{x}_c}\right), \quad \beta, \eta \in \mathbb{R}^d,$$

where λ_c^o are now random effects coming from a $\text{Gamma}(\alpha, \alpha)$ distribution and β is a vector of unknown parameters. The framework is not constrained to parametric forms. Non-parametric intensity models, such

as those using B-splines or Gaussian processes, could be used instead.

For curve-shape parameter prior construction, our choice of the quantity of interest R was motivated by simplicity of the form; one could just as well have used $\frac{G(t_0/2;\theta)}{G(t_0;\theta)}$, albeit with more algebraic manipulations. The general method was aimed at models with monotonically decreasing intensities. If curve-shapes such as Weibull are considered then constructing sensible priors will be more complicated.

In this work, we assumed that we are interested in patient recruitment regardless of the numbers of dropouts observed. In practice, screening failure and patient withdrawal are both prevalent in clinical trials. Assuming the dropouts are independent of the recruitment process, existing survival analysis techniques such as Cox's proportional hazard model (Cox, 1972) or accelerated failure time frailty model (Wei, 1992) could be used in combination with the recruitment model to produce distributions of the numbers of patients in the system at a given time. Such knowledge would be useful to the practitioners and operational researchers in charge of drug-supply chains for the centres.

Anisimov and Fedorov (2007) introduced a method for determining the number of additional centres needed to be open for the study to finish on time. With minimal adaptation, the same method can also be used with our model. However, since it assumes that all new centres are to be opened immediately, it may not apply in all scenarios. We would advocate a simulation-based approach, where forecasts based on different centre opening schedules are compared. As different operational costs can be associated with different schedules, this would become a resource-constrained optimisation problem.

Acknowledgements

This work was supported by the Engineering and Physical Sciences Research Council (grant number EP/L015692/1) and AstraZeneca.

References

- Akaike, H. (1973). Information theory and an extension of the maximum likelihood principle. Petrov BN, Csaki F, editors. Second International Symposium on Information Theory, pages 267–281. Budapest (Hungary): Akademiai Kiado.
- Anisimov, V. V. and Fedorov, V. V. (2007). Modelling, prediction and adaptive adjustment of recruitment in multicentre trials. *Statistics in Medicine*, 26(27):4958–4975.
- Cox, D. R. (1972). Regression models and life-tables. *Journal of the Royal Statistical Society: Series B (Methodological)*, 34(2):187–202.

- Devroye, L. (1986). *Non-uniform Random Variate Generation*. New York: Springer-Verlag.
- Gajewski, B. J., Simon, S. D., and Carlson, S. E. (2008). Predicting accrual in clinical trials with Bayesian posterior predictive distributions. *Statistics in Medicine*, 27(13):2328–2340.
- Gelman, A., Carlin, J. B., Stern, H. S., Dunson, D. B., Vehtari, A., and Rubin, D. B. (2013). *Bayesian data analysis*. Chapman and Hall/CRC.
- Gu, K., Ng, H. K. T., Tang, M. L., and Schucany, W. R. (2008). Testing the ratio of two Poisson rates. *Biometrical Journal: Journal of Mathematical Methods in Biosciences*, 50(2):283–298.
- Heitjan, D. F., Ge, Z., and Ying, G. S. (2015). Real-time prediction of clinical trial enrollment and event counts: a review. *Contemporary Clinical Trials*, 45:26–33.
- Hjort, N. L. and Claeskens, G. (2003). Frequentist model average estimators. *Journal of the American Statistical Association*, 98(464):879–899.
- Huzurbazar, V. S. (1950). Probability distributions and orthogonal parameters. volume 46 of *Mathematical Proceedings of the Cambridge Philosophical Society*, pages 281–284. Cambridge University Press.
- Jiang, Y., Simon, S., Mayo, M. S., and Gajewski, B. J. (2015). Modeling and validating Bayesian accrual models on clinical data and simulations using adaptive priors. *Statistics in Medicine*, 34(4):613–629.
- Kasenda, B., Von Elm, E., You, J., Blümle, A., Tomonaga, Y., Saccilotto, R., Amstutz, A., Bengough, T., Meerpohl, J. J., Stegert, M., et al. (2014). Prevalence, characteristics, and publication of discontinued randomized trials. *JAMA*, 311(10):1045–1052.
- Krishnamoorthy, K. and Thomson, J. (2004). A more powerful test for comparing two Poisson means. *Journal of Statistical Planning and Inference*, 119(1):23–35.
- Lan, Y., Tang, G., and Heitjan, D. F. (2018). Statistical modeling and prediction of clinical trial recruitment. *Statistics in Medicine*, 1–11.
- Lasagna, L. (1979). Problems in publication of clinical trial methodology. *Clinical Pharmacology & Therapeutics*, 25(5part2):751–753.
- Lee, Y. J. (1983). Interim recruitment goals in clinical trials. *Journal of Chronic Diseases*, 36(5):379–389.
- Lindley, D. V. (1957). A statistical paradox. *Biometrika*, 44(1-2):187–192.
- Nelder, J. A. and Mead, R. (1965). A simplex method for function minimization. *The computer journal*, 7(4):308–313.

- Piantadosi, S. and Patterson, B. (1987). A method for predicting accrual, cost, and paper flow in clinical trials. *Controlled Clinical Trials*, 8(3):202–215.
- Robert, C. and Casella, G. (2013). *Monte Carlo statistical methods*. Springer Science & Business Media.
- Robertson, T., Wright, F., and Dykstra, R. (1988). Order restricted statistical inference.
- Schwarz, G. (1978). Estimating the dimension of a model. *The Annals of Statistics*, 6(2):461–464.
- Smith, A. (2013). *Sequential Monte Carlo methods in practice*. Springer Science & Business Media.
- Tang, G., Kong, Y., Chang, C.-C. H., Kong, L., and Costantino, J. P. (2012). Prediction of accrual closure date in multi-center clinical trials with discrete-time Poisson process models. *Pharmaceutical Statistics*, 11(5):351–356.
- Tufts (2013). CSDD impact report - 89% of trials meet enrolment, but timelines slip, half of sites under-enrol. 15(1).
- Wei, L. J. (1992). The accelerated failure time model: a useful alternative to the Cox regression model in survival analysis. *Statistics in Medicine*, 11(14-15):1871–1879.
- Williford, W. O., Bingham, S. F., Weiss, D. G., Collins, J. F., Rains, K. T., and Krol, W. F. (1987). The “constant intake rate” assumption in interim recruitment goal methodology for multicenter clinical trials. *Journal of Chronic Diseases*, 40(4):297–307.
- Zhang, X. and Long, Q. (2010). Stochastic modeling and prediction for accrual in clinical trials. *Statistics in Medicine*, 29(6):649–658.

A Non-parametric bootstrapped test

Algorithm 1: Non-parametric bootstrapped test

input : Series of counts $\{N_c(t)\}_{t=1}^{\tau_c}$, $c = 1, \dots, C$; number of bootstrapped samples B .

output: Probability of observed difference in means under \mathcal{H}_0 .

Calculate observed difference $\Delta = \sum_{c=1}^C \left(\sum_{t=1}^{\tau_c/2} N_c(t) - \sum_{t=\tau_c/2+1}^{\tau_c} N_c(t) \right)$;

for $b \leftarrow 1$ **to** B **do**

for $c \leftarrow 1$ **to** C **do**

 Resample $\{N_c^{(b)}(t)\}_{t=1}^{\tau_c}$ with replacement;

 Calculate difference $\Delta^{(b)} = \sum_{c=1}^C \left(\sum_{t=1}^{\tau_c/2} N_c^{(b)}(t) - \sum_{t=\tau_c/2+1}^{\tau_c} N_c^{(b)}(t) \right)$;

Calculate approximate p -value: $\hat{p} = \frac{1}{B} \sum_{b=1}^B \mathbb{I}_{\{\Delta \geq \Delta^{(b)}\}}$

B Curve-shape

The integrated, normalised parametric intensities are:

$$\begin{aligned} G_0(t) &= t, \\ G_1(t; \theta) &= \frac{\log(1 + \theta t)}{\log(1 + \theta \tau)} \tau, \\ G_\kappa(t; \theta) &= \frac{(1 + \theta t/\kappa)^{1-\kappa} - 1}{(1 + \theta \tau/\kappa)^{1-\kappa} - 1} \tau, \quad \kappa \notin \{0, 1, \infty\}, \\ G_\infty(t; \theta) &= \frac{1 - e^{-\theta t}}{1 - e^{-\theta \tau}} \tau. \end{aligned}$$

C Maximum likelihood inference

In the frequentist setting, we aim to find estimators which maximise the likelihood surface (2). This is equivalent to maximising the log-likelihood surface (up to a constant)

$$\begin{aligned} \ell(\alpha, \phi, \theta | \mathbf{n}, \tau) &= C \left(\alpha \log \frac{\alpha}{\phi} - \log \Gamma(\alpha) \right) - \sum_{c=1}^C \left[\left(\alpha + n_c^{(\cdot)} \right) \log \left(G(\tau_c; \theta) + \frac{\alpha}{\phi} \right) \right. \\ &\quad \left. - \log \Gamma \left(\alpha + n_c^{(\cdot)} \right) - \sum_{t=1}^{\tau_c} n_c^{(t)} \log(G(t; \theta) - G(t-1; \theta)) \right]. \end{aligned}$$

The log-likelihood function can be optimised using a range of methods, for example, the Nelder-Mead (Nelder and Mead, 1965) method used in R. The inverse of the negative Hessian at the mode can then be used as the covariance matrix for the asymptotic normal distribution of the MLEs.

The α and ϕ parameters are asymptotically orthogonal for a homogeneous Poisson-gamma model

(Huzurbazar, 1950). A time contraction argument can be used to extend the result to the inhomogeneous case. As discussed in Section 4 and visible from (3), in the special case where $\tau_c \equiv \tau \forall c$, θ is orthogonal to both α and ϕ . When carrying out maximum likelihood inference, different model selection criteria such as AIC (Akaike, 1973) and BIC (Schwarz, 1978) can be used. Alternatively, one could employ frequentist model averaging methods (see (Hjort and Claeskens, 2003), for instance).

The score function and the observed and expected information are provided in the Supplementary Material. The only pair of parameters which are not asymptotically orthogonal when centres have not been open for the same length of time are ϕ and θ .

D Curve-shape prior

The flexible form (4), leads to the following prior density for $\tilde{\theta}$,

$$\pi_0(\tilde{\theta}|\kappa, a, b) = \begin{cases} t_0 \exp\{\tilde{\theta} - t_0 e^{\tilde{\theta}}\} f_B(\exp\{-t_0 e^{\tilde{\theta}}\}; a, b), & \kappa = \infty \\ t_0 e^{\tilde{\theta}} (1 + t_0 e^{\tilde{\theta}}/\kappa)^{-\kappa-1} f_B\left(\left(1 + t_0 e^{\tilde{\theta}}/\kappa\right)^{-\kappa}; a, b\right), & \kappa \in (0, \infty) \end{cases}, \quad \theta > 0,$$

where $f_B(\cdot; a, b)$ is a density of a beta variate with shape parameters a and b .

E Sampling time to completion via model averaging

In (Lan et al., 2018), the time is sampled by repeatedly simulating the whole system until the condition is satisfied, which is inefficient and only provides an approximate distribution due to the discretisation in the time domain. To sample the time to completion exactly, we use the integrated intensity function of the whole trial $\Lambda(t)$. If T is the time to the m th arrival of an inhomogeneous Poisson process with integrated intensity $\Lambda(t)$ then (Devroye, 1986)

$$\Lambda(T) \sim \text{Gamma}(m, 1).$$

Given (α, β, θ) , we can sample rates the λ_c^o for all the centres and construct one realisation of the integrated intensity Λ for the whole trial. Then, to obtain a single realisation of T , we sample a $\text{Gamma}(m, 1)$ variate and use an inverse-transform of Λ on it. Unless all the centres had been open for the same length of time, the inversion procedure will involve some root-finding algorithm, such as Newton-Raphson. As $\Lambda(t)$ in our framework is a monotonically increasing function, the non-linear equation will have a unique solution. Parameter uncertainty can be incorporated into this predictive by using a different sample from the posterior at each iteration.

Given C^+ centres with the first C already opened before the census time and the remaining $C^+ - C$ to

be open, as well as known centre opening times $t_0^{(c)}$, $c = 1, \dots, C^+$, we construct the integrated intensity for modelling the recruitment since the census time τ ,

$$\Lambda(t) = \sum_{c=1}^C \lambda_c^o \left[G(t - t_0^{(c)}; \theta) - G(\tau_c; \theta) \right] + \sum_{c=C+1}^{C^+} \lambda_c^o G(t - t_0^{(c)}; \theta) \mathbb{I}_{\{t > t_0^{(c)}\}}, \quad t \geq \tau,$$

where $\mathbb{I}_{\{\cdot\}}$ is the indicator function and

$$\lambda_c^o | \alpha, \phi, \theta, \mathbf{n} \sim \begin{cases} \text{Gamma}(\alpha + n_c^{(\cdot)}, \alpha/\phi + G(\tau_c; \theta)), & c = 1, \dots, C \\ \text{Gamma}(\alpha, \alpha/\phi), & c = C + 1, \dots, C^+ \end{cases}. \quad (12)$$

Algorithm 2 outlines the sampling procedure to obtain the distribution of the time needed to recruit the target number of patients m .

Algorithm 2: Model-averaged time to completion sampling

input : Models $\mathcal{M}_1, \dots, \mathcal{M}_k$ with posterior probabilities $\pi(\mathcal{M}_1 | \mathbf{n}), \dots, \pi(\mathcal{M}_k | \mathbf{n})$ and posterior samples from each model, number of samples from the predictive B , target number of recruitments m

output: Distribution of the time to completion $\{T^{(b)}\}_{b=1}^B$

for $b \leftarrow 1$ **to** B **do**

Sample $\mathcal{M}^{(b)} \sim \pi(\mathcal{M}_k | \mathbf{n})$;
Sample $(\alpha, \phi, \theta)^{(b)} \sim \pi(\alpha, \phi, \theta | \mathcal{M}^{(b)}, \mathbf{n})$;
Sample rates $\lambda_c^o | (\alpha, \phi, \theta)^{(b)}$ from distributions (12) and construct $\Lambda^{(b)}(t)$;
Sample $\tilde{T} \sim \text{Gamma}(m, 1)$ and solve $\Lambda^{(b)}(T) = \tilde{T}$;
Set $T^{(b)} = T$;

SUPPLEMENTARY MATERIAL

Supplementary material for “Interim recruitment prediction for multi-centre clinical trials” which includes material on

- Curve-shape identifiability
- Bayesian inference
- Importance sampling
- Additional details from the simulation study
- Score and observed and expected information of the model

Curve-shape identifiability

In two instances, the flexible-tail form can give rise to identifiability problems:

$$\underline{t, \tau \gg \kappa/\theta \text{ and } \kappa < 1}$$

$$G_\kappa(t; \theta) = \frac{(1 + \theta t/\kappa)^{1-\kappa} - 1}{(1 + \theta \tau/\kappa)^{1-\kappa} - 1} \tau \approx \frac{(\theta t/\kappa)^{1-\kappa} - 1}{(\theta \tau/\kappa)^{1-\kappa} - 1} \tau \approx \left(\frac{t}{\tau}\right)^{1-\kappa} \tau,$$

which does not depend on θ .

$$\underline{t, \tau \gg \kappa/\theta \text{ and } \kappa \gg 1}$$

$$\begin{aligned} G_\kappa(t; \theta) &= \frac{(1 + \theta t/\kappa)^{1-\kappa} - 1}{(1 + \theta \tau/\kappa)^{1-\kappa} - 1} \tau \\ &\approx \frac{(1 + \theta t/\kappa)e^{-\theta t} - 1}{(1 + \theta \tau/\kappa)e^{-\theta \tau} - 1} \tau \\ &\approx \frac{e^{-\theta t} - 1}{e^{-\theta \tau} - 1} \tau, \end{aligned}$$

which does not depend on κ .

Bayesian inference

For a general model with data y , parameter vector $\psi \in \Omega$ and likelihood $f(y|\psi)$, we assign a prior density or mass function to ψ , $\pi_0(\psi)$. Inference is based on the posterior distribution, obtained by the Bayes’s rule,

$$\pi(\psi|y) = \frac{f(y|\psi)\pi_0(\psi)}{\int_\Omega f(y|\psi)\pi_0(\psi) \, d\psi}, \quad \psi \in \Omega.$$

Often times, the marginal likelihood of the data $p(y) = \int_\Omega f(y|\psi)\pi_0(\psi) \, d\psi$ is not tractable and so Monte Carlo sampling methods need to be employed to obtain samples from the posterior. Strictly, the marginal

likelihood, $p(y)$ is $p(y|\mathcal{M})$ the probability of the data given the choice of model, encapsulated in f . Consider, now, a range of models $\mathcal{M}_1, \dots, \mathcal{M}_K$ with associated prior probabilities $\pi_0(\mathcal{M}_k)$, $k = 1, \dots, K$. Using Bayes's rule, we obtain the posterior model probabilities, up to a proportionality constant,

$$\pi(\mathcal{M}_k|y) \propto p(y|\mathcal{M}_k)\pi_0(\mathcal{M}_k), \quad k = 1, \dots, K.$$

Importance sampling

Multiplying the priors and the likelihood we obtain the posterior distribution for the parameters up to a proportionality constant. Since the dimension of the parameter space is not large, we can sample from the posterior by the means of importance sampling.

For any function of interest $h(\psi)$,

$$\begin{aligned} \mathbb{E}[h(\psi)] &= \int_{\Omega} h(\psi)\pi_p(\psi|y) \, d\psi = \frac{\int_{\Omega} h(\psi)\omega(\psi)q(\psi) \, d\psi}{\int_{\Omega} f(y|\psi)\pi_0(\psi) \, d\psi} \\ &\approx \frac{\sum_{b=1}^B h(\psi^{(b)})\omega(\psi^{(b)})}{\sum_{b=1}^B \omega(\psi^{(b)})}, \end{aligned}$$

where $\psi^{(b)}$, $b = 1, \dots, B$ are samples from a proposal distribution q with unnormalised weights

$$\omega(\psi) = \frac{f(y|\psi)\pi_0(\psi)}{q(\psi)}.$$

The marginal likelihood may be approximated by

$$\hat{p}(y) = \frac{1}{B} \sum_{b=1}^B \omega(\psi^{(b)}).$$

This is an unbiased estimate which can be used for model selection or model averaging.

The efficiency of the sampling procedure depends on the choice of proposal distribution q and the may be measured using the effective sample size (ESS),

$$\text{ESS} = \frac{\left(\sum_{b=1}^B \omega(\psi^{(b)})\right)^2}{\sum_{b=1}^B \omega(\psi^{(b)})^2}.$$

If the proposal distribution closely resembles the true posterior, then all the weights will be roughly the same resulting in the ESS being close to M . On the other extreme, if the proposal badly captures the posterior and one sample's weight dominates the others, then ESS will be close to one.

If $\psi^{(b)}$ are resampled with replacement with probabilities proportional to the weights, then the resulting sample, say $\{\psi_*^{(b)}\}_{b=1}^B$, will have the distribution approximating π . The new sample is used when sampling from the predictive distribution to marginalise over the parameter posterior.

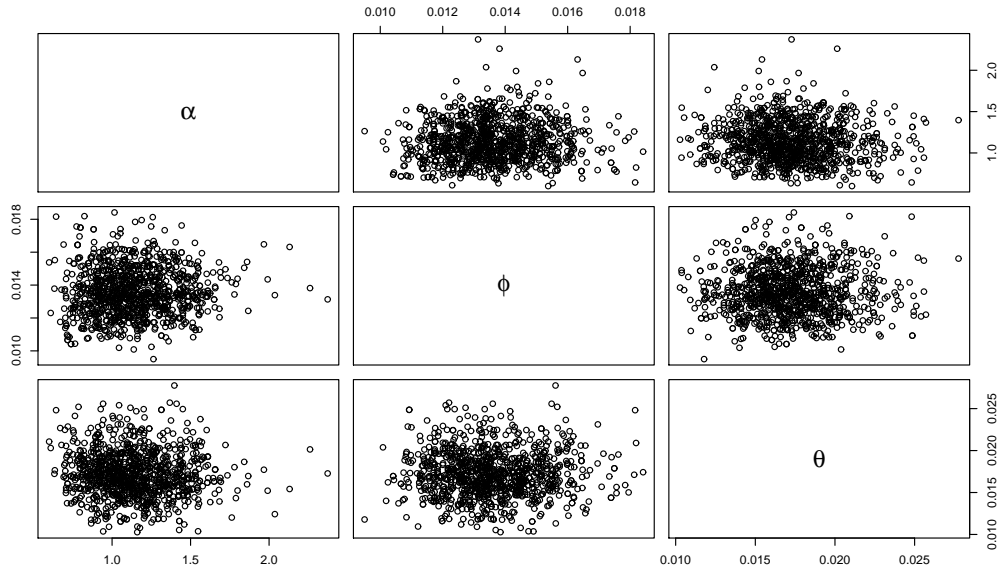


Figure 1: Matrix scatterplot of the parameter posterior of the model with highest posterior probability.

Additional details from the simulation study

Figure 1 shows the plots of posterior samples of the model. The three parameters are close to orthogonal as discussed in Sections 4 and 5.1, and this approximate independence was also observed in the posteriors of other models.

Figure 2 shows a QQ-plot of the hierarchical gamma distribution compared to the posterior means of the random effects. The approximately straight line indicates that generating rates for newly opened centres from the gamma distribution will be consistent with what has been observed thus far. Figure 3 shows a QQ-plot of the theoretical, negative binomial distribution of recruitments in the first 2 months compared the observed distribution ($t_* = 60$). The theoretical distribution used the posterior means of the parameters, and the prior random effect distribution was used. The straight line shows that the model can predict the recruitment in the first two months of a centre sufficiently well. In practice, the two diagnostics would indicate that the mixing gamma distribution is sufficient and that the model is capable of accurately predicting recruitments in the early days of a new centre.

Figures 4, 5, 6 and 7 show the diagnostic plots for models fit to simulated datasets at the census $t = 360$ with the true random-effect distribution being a mixture. For $\mathbb{E}[\lambda_c^o] = 0.01$, the relationship is close to linear and is reflected in the reasonably accurate predictions shown in the article. The QQ-plots for $\mathbb{E}[\lambda_c^o] = 0.03$ show stronger non-linearity and informing us of the potential misspecification, thus showing that the diagnostics can be used to validate the model.

Figures 8a and 8b show examples of recruitment predictions when the random effects have a mixture

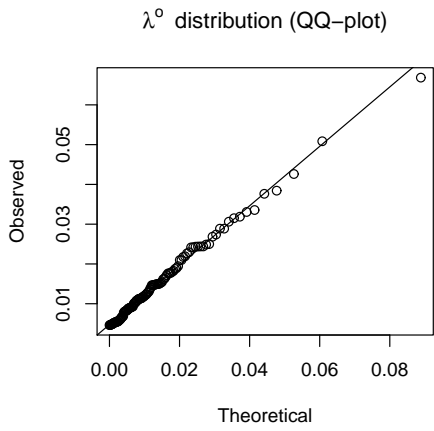


Figure 2: Re-estimated λ_c^o expectations compared to $\text{Gamma}(\hat{\alpha}, \hat{\alpha}/\hat{\phi})$ distribution.

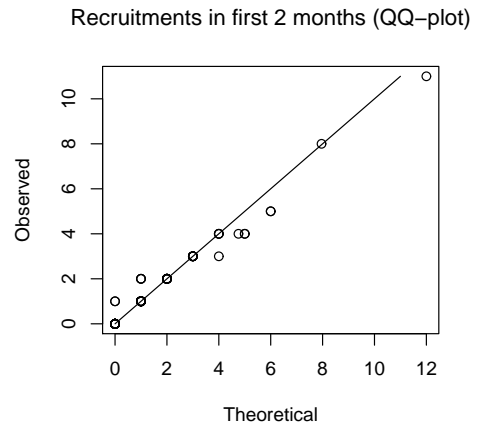


Figure 3: Observed recruitments compared to the theoretical negative binomial distribution.

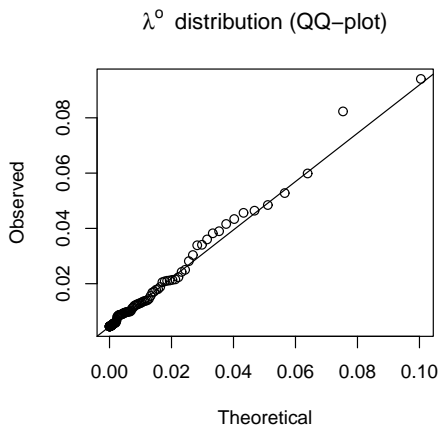


Figure 4: Re-estimated λ_c^o expectations compared to $\text{Gamma}(\hat{\alpha}, \hat{\alpha}/\hat{\phi})$ distribution; true random-effect distribution is a mixture with $\mathbb{E}[\lambda_c^o] = 0.01$.

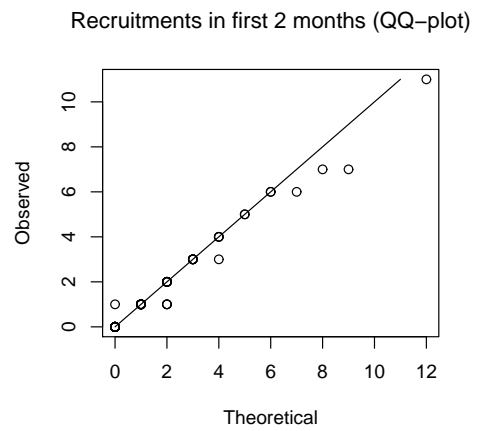


Figure 5: Observed recruitments compared to the theoretical negative binomial distribution; true random-effect distribution is a mixture with $\mathbb{E}[\lambda_c^o] = 0.01$.

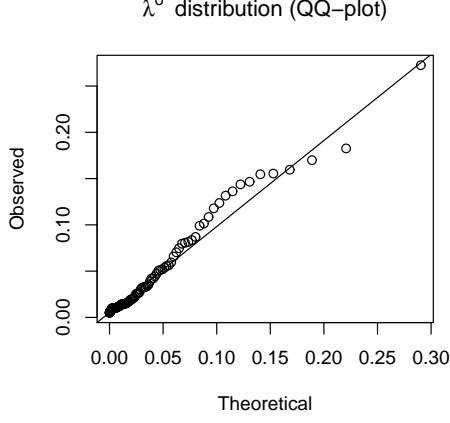


Figure 6: Re-estimated λ_c^o expectations compared to $\text{Gamma}(\hat{\alpha}, \hat{\alpha}/\hat{\phi})$ distribution; true random-effect distribution is a mixture with $\mathbb{E}[\lambda_c^o] = 0.03$.

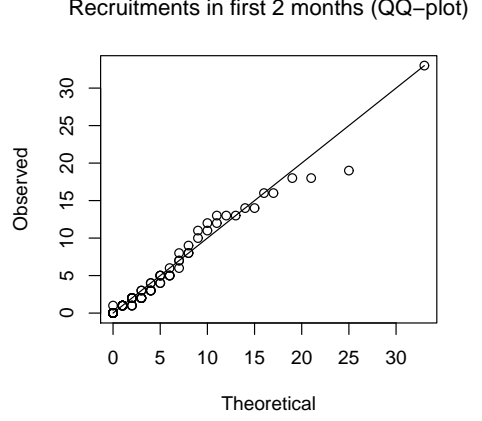


Figure 7: Observed recruitments compared to the theoretical negative binomial distribution; true random-effect distribution is a mixture with $\mathbb{E}[\lambda_c^o] = 0.03$

distribution and the centre opening times are “clumped” together. The clumping accentuates the effect of the misspecification; the fitted model relies on the “incorrect” prior gamma distribution when simulating rates for unopened centres.

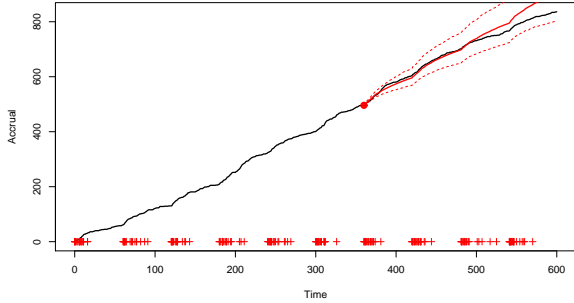
Figures 9a and 9b show the predictions made when using data simulated from a Weibull-shape intensity with centre opening times clumped together. With repeated simulations, we found a consistent correspondence between linear QQ-plots and accurate predictions.

Score and observed and expected information

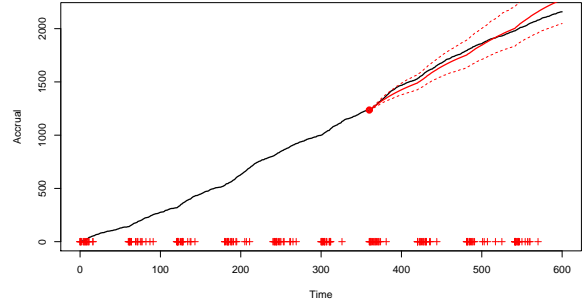
Here we provide the score function and the observed and expected information, for frequentist inference.

The score function is the gradient of the log-likelihood of the model (as presented in Appendix C),

$$\begin{aligned} \nabla \ell(\alpha, \phi, \theta | \mathbf{n}, \boldsymbol{\tau}) &= \\ &= \begin{bmatrix} C \left(1 + \log \frac{\alpha}{\phi} - \psi(\alpha) \right) - \sum_{c=1}^C \left(\frac{\alpha + n_c^{(\cdot)}}{\alpha + \phi G(\tau_c; \theta)} + \log \left(G(\tau_c; \theta) + \frac{\alpha}{\phi} \right) - \psi \left(\alpha + n_c^{(\cdot)} \right) \right) \tau \\ -C\alpha/\phi + \sum_{c=1}^C \frac{\alpha(\alpha + n_c^{(\cdot)})}{\phi(\alpha + \phi G(\tau_c; \theta))} \tau \\ - \sum_{c=1}^C \left[\partial_\theta G(\tau_c; \theta) \left(\frac{\alpha + n_c^{(\cdot)}}{G(\tau_c; \theta) + \frac{\alpha}{\phi}} \right) - \sum_{t=1}^{\tau_c} n_c^{(t)} \left(\frac{\partial_\theta G(t; \theta) - \partial_\theta G(t-1; \theta)}{G(t; \theta) - G(t-1; \theta)} \right) \right] \end{bmatrix}. \end{aligned}$$

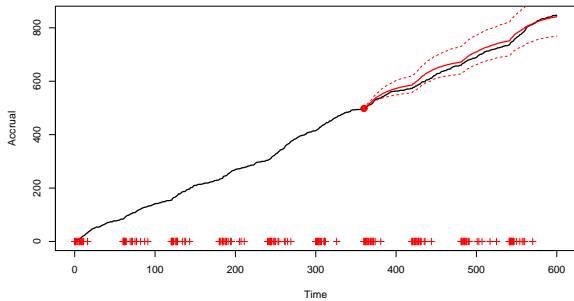


(a) Clumped openings, $\mathbb{E}[\lambda_c^o] = 0.01$;
 p -value = 0.666

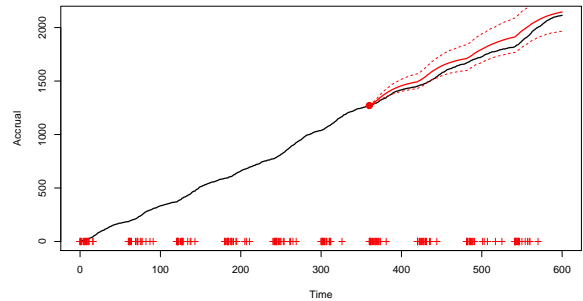


(b) Clumped openings, $\mathbb{E}[\lambda_c^o] = 0.03$;
 p -value = 0.312

Figure 8: Accruals (black, solid) with predictive means (red, solid) and 95% prediction bands (red, dashed) when the true random-effect distribution is a mixture, in various scenarios. Prediction bands are based on the 2.5% and 97.5% quantiles. The “+” symbols on the abscissa indicate centre opening times.



(a) Clumped openings, $\mathbb{E}[\lambda_c^o] = 0.01$;
 p -value = 0.294



(b) Clumped openings, $\mathbb{E}[\lambda_c^o] = 0.03$;
 p -value = 0.064

Figure 9: Accruals (black, solid) with predictive means (red, solid) and 95% prediction bands (red, dashed) when the true intensity shape is Weibull and opening times are clumped, with two different values for $\mathbb{E}[\lambda_c^o]$. Prediction bands are based on the 2.5% and 97.5% quantiles. The “+” symbols on the abscissa indicate centre opening times.

The observed information matrix is made up of the negative Hessian elements

$$\begin{aligned}
-\partial_{\alpha\alpha}^2 \ell(\alpha, \phi, \theta | \mathbf{n}, \boldsymbol{\tau}) &= C \left(\psi'(\alpha) - \frac{1}{\alpha} \right) + \sum_{n=1}^C \left(\frac{\phi G(\tau_c; \theta) - n_c^{(\cdot)} + 1}{\alpha + \phi G(\tau_c; \theta)} - \psi'(\alpha + n_c^{(\cdot)}) \right), \\
-\partial_{\phi\phi}^2 \ell(\alpha, \phi, \theta | \mathbf{n}, \boldsymbol{\tau}) &= -C\alpha/\phi^2 + \sum_{c=1}^C \frac{\alpha(\alpha + 2\phi G(\tau_c; \theta))(\alpha + n_c^{(\cdot)})}{\phi^2[\alpha + \phi G(\tau_c; \theta)]^2}, \\
-\partial_{\theta\theta}^2 \ell(\alpha, \phi, \theta | \mathbf{n}, \boldsymbol{\tau}) &= \sum_{c=1}^C \left[\frac{(\alpha + n_c^{(\cdot)}) [\partial_{\theta\theta}^2 G(\tau_c; \theta)(G(\tau_c; \theta) + \alpha/\phi) - (\partial_{\theta} G(\tau_c; \theta))^2]}{[G(\tau_c; \theta) + \alpha/\phi]^2} \right. \\
&\quad \left. - \sum_{t=1}^{\tau_c} n_c^{(t)} \frac{H_t \partial_{\theta\theta}^2 H_t - (\partial_{\theta} H_t)^2}{(H_t)^2} \right], \\
-\partial_{\alpha\phi}^2 \ell(\alpha, \phi, \theta | \mathbf{n}, \boldsymbol{\tau}) &= \frac{1}{\phi} \left(C - \sum_{c=1}^C \frac{\alpha^2 + 2\alpha\phi G(\tau_c; \theta) + \phi G(\tau_c; \theta)n_c^{(\cdot)}}{[\alpha + \phi G(\tau_c; \theta)]^2} \right), \\
-\partial_{\alpha\theta}^2 \ell(\alpha, \phi, \theta | \mathbf{n}, \boldsymbol{\tau}) &= \sum_{c=1}^C \partial_{\theta} G(\tau_c; \theta) \frac{G(\tau_c; \theta) - n_c^{(\cdot)}/\phi}{[G(\tau_c; \theta) - \alpha/\phi]^2}, \\
-\partial_{\phi\theta}^2 \ell(\alpha, \phi, \theta | \mathbf{n}, \boldsymbol{\tau}) &= -\alpha \sum_{c=1}^C \partial_{\theta} G(\tau_c; \theta) \frac{\alpha + n_c^{(\cdot)}}{[\alpha + \phi G(\tau_c; \theta)]^2},
\end{aligned}$$

where $\psi(x) = \Gamma'(x)/\Gamma(x)$ and $H_t = G(t; \theta) - G(t-1; \theta)$ to simplify the notation. Noting that $\mathbb{E}[N_c^{(\cdot)}] = \phi G(\tau_c; \theta)$, we obtain the entries of the Fisher information matrix,

$$\begin{aligned}
\mathbb{E}[-\partial_{\alpha\alpha}^2 \ell(\alpha, \phi, \theta | \mathbf{N}, \boldsymbol{\tau})] &= C \left(\psi'(\alpha) - \frac{1}{\alpha} \right) + \sum_{n=1}^C \left(\frac{1}{\alpha + \phi G(\tau_c; \theta)} - \mathbb{E}[\psi'(\alpha + n_c^{(\cdot)})] \right), \\
\mathbb{E}[-\partial_{\phi\phi}^2 \ell(\alpha, \phi, \theta | \mathbf{N}, \boldsymbol{\tau})] &= \frac{\alpha}{\phi} \sum_{c=1}^C \frac{G(\tau_c; \theta)}{\alpha + \phi G(\tau_c; \theta)}, \\
\mathbb{E}[-\partial_{\theta\theta}^2 \ell(\alpha, \phi, \theta | \mathbf{N}, \boldsymbol{\tau})] &= \sum_{c=1}^C \left[\frac{\phi (\partial_{\theta\theta}^2 G(\tau_c; \theta)(G(\tau_c; \theta) + \alpha/\phi) - (\partial_{\theta} G(\tau_c; \theta))^2)}{\phi G(\tau_c; \theta) + \alpha} \right. \\
&\quad \left. - \sum_{t=1}^{\tau_c} n_c^{(t)} \partial_{\theta\theta}^2 H_t - \frac{(\partial_{\theta} H_t)^2}{H_t} \right], \\
\mathbb{E}[-\partial_{\alpha\phi}^2 \ell(\alpha, \phi, \theta | \mathbf{N}, \boldsymbol{\tau})] &= 0, \\
\mathbb{E}[-\partial_{\alpha\theta}^2 \ell(\alpha, \phi, \theta | \mathbf{N}, \boldsymbol{\tau})] &= 0, \\
\mathbb{E}[-\partial_{\phi\theta}^2 \ell(\alpha, \phi, \theta | \mathbf{N}, \boldsymbol{\tau})] &= -\alpha \sum_{c=1}^C \frac{\partial_{\theta} G(\tau_c; \theta)}{\alpha + \phi G(\tau_c; \theta)}.
\end{aligned}$$